The angularly resolved O 1s ion-yield spectrum of O_2 revisited

R. Püttner and K. Ueda

Citation: J. Chem. Phys. **145**, 224302 (2016); doi: 10.1063/1.4971240

View online: http://dx.doi.org/10.1063/1.4971240

View Table of Contents: http://aip.scitation.org/toc/jcp/145/22

Published by the American Institute of Physics

The angularly resolved O 1*s* ion-yield spectrum of O_2 revisited

R. Püttner[1,a] and K. Ueda[2]
[1]*Fachbereich Physik, Freie Universität Berlin, Arnimallee 14, D-14195 Berlin-Dahlem, Germany*
[2]*Institute of Multidisciplinary Research for Advanced Materials, Tohoku University, Sendai 980-8577, Japan*

(Received 8 September 2016; accepted 17 November 2016; published online 8 December 2016)

The high-resolution photoabsorption spectrum of O_2 below the O $1s\sigma^{-1}$ ionization threshold has been reanalyzed by using a sophisticated fit approach. For the vibrational substates of the O $1s\sigma_u^{-1}(^4\Sigma_u^-)3s\sigma_g(^3\Sigma_u^-)$ Rydberg state Fano lineshapes are observed indicating an interaction with the O $1s\sigma_g^{-1}(^4\Sigma_g^-)3\sigma_u^*(^3\Sigma_u^-)$ core-to-valence excited state. In the angularly resolved ion-yield spectrum recorded at 90° relative to the polarization direction of the synchrotron radiation clear evidence for the O $1s\sigma_g^{-1}(^2\Sigma_g^-)3\sigma_u^*(^3\Sigma_u^-)$ and the O $1s\sigma_u^{-1}(^2\Sigma_u^-)3s\sigma_g(^3\Sigma_u^-)$ state was found. This observation clearly suggests that Λ, the projection of total orbital angular momentum on the molecular axis, is not well separated in the angularly resolved ion-yield spectrum due to a partial breakdown of the axial-recoil approximation for these transitions. *Published by AIP Publishing.* [http://dx.doi.org/10.1063/1.4971240]

I. INTRODUCTION

The photoabsorption spectrum of O_2 below the O $1s\sigma^{-1}$ ionization threshold is known to be very complex, mainly because of two reasons. First, O_2 in its ground state has an open-shell structure and a total wave-function with a $^3\Sigma_g^-$ symmetry. This leads in case of a O $1s\sigma^{-1}$ core ionization to an interaction of the spins of the valence electrons and of the remaining core electron, and as a result to the two ionization thresholds O $1s\sigma^{-1}$ $(^2\Sigma^-)$ and O $1s\sigma^{-1}$ $(^4\Sigma^-)$ split by ≅1.04 eV.[1] According to calculations both these thresholds are further split by 7 meV and 50 meV, respectively, into the components (Σ_g^-) and (Σ_u^-).[1] Second, the antibonding resonance O $1s\sigma_g^{-1}3\sigma_u^*(^3\Sigma_u^-)$ is—contrary to most of the other molecules—lying below the ionization threshold and interacts strongly with the Rydberg states.

This complexity initiated numerous experimental and theoretical investigations in the last three decades. Over this period the photoabsorption spectra have been measured by several groups using an experimental resolution that improved considerably with time.[2–6] Beside this, some groups recorded symmetry-resolved photoabsorption spectra,[7–10] resonant Auger spectra,[6,10–14] or performed resonant inelastic X-ray scattering (RIXS).[15,16] These studies were complemented by more and more sophisticated theoretical studies.[6–8,17] All these studies allowed a general understanding of the photoabsorption spectrum; however, some details are still not fully explained.

Interestingly, none of the above mentioned extensive studies performed a detailed fit analysis of the photoabsorption spectra. In the present approach we fill this gap by fitting both, the total ion-yield spectrum and the angularly resolved partial ion-yield spectra; in this way a number of new details were identified. For example, we observed Fano lineshapes, which are likely due to the interaction of a bound Rydberg state and the dissociative O $1s\sigma_g^{-1}3\sigma_u^*(^3\Sigma_u^-)$ resonance. We also found that the O $1s\sigma_g^{-1}3\sigma_u^*(^3\Sigma_u^-)$ and the O $1s\sigma_u^{-1}3s\sigma_g(^3\Sigma_u^-)$ core-to-valence excitations are present in the ion yield spectrum measured at 90°. This is not in line with the photoabsorption selection rules for the projection of the total orbital angular momentum on the molecular axis, Λ. To angularly resolved ion-yield spectra they are only applicable if the axial-recoil approximation is valid, which is generally assumed to be the case. As a consequence, the present findings suggest a breakdown of the axial-recoil approximation for these excitations.

Besides these new findings, the present study confirms generally the assignments given by Tanaka *et al.*[10] based on symmetry-resolved photoabsorption and resonant Auger spectra. However, we also show that some of the spectral features assigned by Tanaka *et al.*[10] show additional contributions, which were not taken into account before.

II. EXPERIMENTAL SPECTRA, DATA ANALYSIS, AND RESULTS

The O_2 molecule possesses 16 electrons resulting in the ground-state configuration $1\sigma_g^2 1\sigma_u^{*2} 2\sigma_g^2 2\sigma_u^{*2} 3\sigma_g^2 1\pi_g^4 1\pi_u^{*2} 3\sigma_u^{*0}(^3\Sigma_g^-)$. Here, the molecular orbitals $1\sigma_g$ $(2\sigma_g)$ and $1\sigma_u^*$ $(2\sigma_u^*)$ are mainly formed by the two O 1*s* (O 2*s*) atomic orbitals, while the molecular orbitals $3\sigma_g$, $1\pi_g$, $1\pi_u^*$, and $3\sigma_u^*$ are formed by the six O 2*p* atomic orbitals. The "∗" indicates the antibonding character of the orbitals.

Figure 1 shows the total ion-yield spectrum of O_2 below the O $1s\sigma^{-1}$ threshold, consisting of the excitations O $1s\sigma_g^{-1}3\sigma_u^*(^3\Sigma_u^-)$, O $1s\sigma^{-1}Ryd(^3\Sigma_u^-)$, and O $1s\sigma^{-1}Ryd(^3\Pi_u)$. This spectrum was recorded at the soft x-ray PLEIADES beamline[18] dedicated to the spectroscopy of isolated species at the SOLEIL Synchrotron in Saint-Aubin, France. The beamline optics has been optimized for ultrahigh spectral resolution, to routinely achieve resonant photoemission measurements in the sub-lifetime regime.[19–22] The photon bandwidth achieved is about 23 meV. The solid line through the data points

[a]Electronic address: puettner@zedat.fu-berlin.de

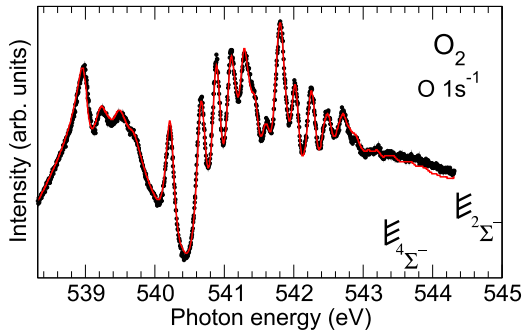

FIG. 1. The total ion-yield spectrum of O_2 below the O $1s\sigma^{-1}$ ionization threshold (see Section II for details). The solid line through the data points indicates the results of a simple fit approach, see text.

represents the results of a simple fit approach which uses the fit results obtained for the 0° and the 90° spectrum, see below, each multiplied with one weight factor.

As shown by Feifel *et al.*,[6] a description of this energy region in a diabatic model leads to a strongly dominating broad peak with a width of approximately 4 eV, i.e., over the entire energy range, due to the excitation to the antibonding $3\sigma_u^*$ orbital as well as to minor contributions of excitations to the Rydberg orbitals. Contrary to these results obtained within the diabatic approach, the experimental spectrum is dominated in the energy range below 540.5 eV by a broad peak with a width of approximately 1.5 eV, and in the range above this value by narrow lines. These findings can only be explained by a strong interaction of the O $1s\sigma_g^{-1}3\sigma_u^*(^3\Sigma_u^-)$ state and the O $1s\sigma^{-1}Ryd(^3\Sigma_u^-)$ states. This interaction explains both the narrowing of the O $1s\sigma_g^{-1}3\sigma_u^*(^3\Sigma_u^-)$ excitation from 4 eV in the diabatic model to 1.5 eV in the experimental spectrum and the strong intensity borrowing for the O $1s\sigma^{-1}Ryd$ excitations. In this situation the adiabatic approach is much more appropriate than the diabatic approach. The interaction also renders the understanding of the spectra highly complicated.

However, for a full understanding of the O 1*s* photoabsorption spectrum, one has to take into account that there are two types of Rydberg-valence mixing, which are described in the textbook of Lefebvre-Brion and Field.[24] In the first type of interaction "the configurations of the Rydberg and the valence states differ by two orbitals."[24] This type of mixing is weak, and can be described with both the diabatic and adiabatic pictures. As written in Ref. 24 "in the adiabatic approximation, an electrostatic interaction takes place and mixes the vibrational levels of these two states. In the adiabatic representation, the coefficients of the two configurations vary with the (internuclear distance) *R*." The fact that two different descriptions are appropriate for this case is discussed in more detail by Jasper *et al.*[25] In the second type of interaction "the configurations of the Rydberg and the valence states differ by only one orbital."[24] In this case the interaction is much stronger and only the adiabatic approximation is appropriate. As said in Ref. 24 "in this picture, only the orbital, not the configuration mixing coefficients, changes with *R*."

Interestingly, core-excited O_2 exhibits both types of Rydberg-valence mixing due to the *gerade* and *ungerade* symmetries of the O 1*s* core orbitals. Based on the dipole selection rules for molecules with inversion symmetry the parity is changed by the excitation, i.e., $g \rightarrow u$ or $u \rightarrow g$. Because of this, the valence orbital $3\sigma_u^*$ can only be populated from the O $1s\sigma_g^{-1}$ core orbital. The same holds for the $np\lambda_u$ Rydberg orbitals, so that the Rydberg-valence mixing between the core-excited states O $1s\sigma_g^{-1}3\sigma_u^*$ and O $1s\sigma_g^{-1}np\lambda_u$ is of type 2. This type of mixing is the origin for the narrowing of the O $1s\sigma_g^{-1}3\sigma_u^*$ resonance from 4 eV in the diabatic representation to 1.5 eV in the adiabatic approximation as described in the previous paragraph. Contrary to this, the $ns\lambda_g$ and $nd\lambda_g$ Rydberg orbitals can only be populated from the O $1s\sigma_u^{-1}$ core orbital leading to a much weaker Rydberg-valence mixing of type 1. The present study will shed light on this weak type 1 mixing.

As mentioned above, the main idea of the present study was to understand the photoabsorption spectrum of O_2 on the basis of a fit analysis. Due to the complexity of the spectrum caused by various effects partially discussed above, different parts of the spectrum are described with different models. Although the models are mainly based on physical ideas, they are partially also *ad hoc* approaches in order to estimate in the fit analysis the contributions of some of the spectral features, and to separate them from the contributions of other spectral features.

In the following we shall first present the angularly resolved ion-yield spectra taken at 0° and 90° relative to the polarization of the synchrotron radiation, see Figs. 2(a) and 2(b), respectively. These spectra have been taken from Ref. 10, which also describes the technique used to record them. In brief, the angularly resolved ion-yield spectra were measured at beamline 27SU of the synchrotron radiation facility SPring8 using two identical retarding-potential-type ion detectors.[23] These detectors were mounted to detect fragment ions emitted parallel or perpendicular to the polarization direction of the light. A retarding potential of 6 V has been applied to each detector for detecting ions with kinetic energies larger than 6 eV. The energy calibration of all spectra is also taken from Ref. 10, with an accuracy of 40 meV for the photon energy scale.

The angularly resolved ion-yield spectra in Figs. 2(a) and 2(b) exhibit a simpler structure than the total ion-yield spectrum since—based on Λ being a good quantum number —the selection rules $\Delta\Lambda = 0$ and $\Delta\Lambda = \pm 1$ can be derived for the 0° and 90° spectra, respectively. These selection rules in combination with the $^3\Sigma$ symmetry of the total ground state wavefunction should lead solely to states with $^3\Sigma$ symmetry for the total wavefunction in the 0° spectrum and with $^3\Pi$ symmetry in the 90° spectrum. We will show that, in the present angularly resolved spectra, these expectations are not strictly fulfilled for some excitations due to partial breakdown of the axial recoil approximation. The detailed fit models for the individual spectral regions of the angularly resolved spectra will be described together with the discussion.

A. The 0° spectrum

1. The O $1s\sigma_g^{-1}3\sigma_u^*(^3\Sigma_u^-)$ and O $1s\sigma_u^{-1}3s\sigma_g(^3\Sigma_u^-)$ excitations

The region between 538 and 540.5 eV is dominated by a broad peak caused by the O $1s\sigma_g^{-1}3\sigma_u^*(^3\Sigma_u^-)$ excitation. On top

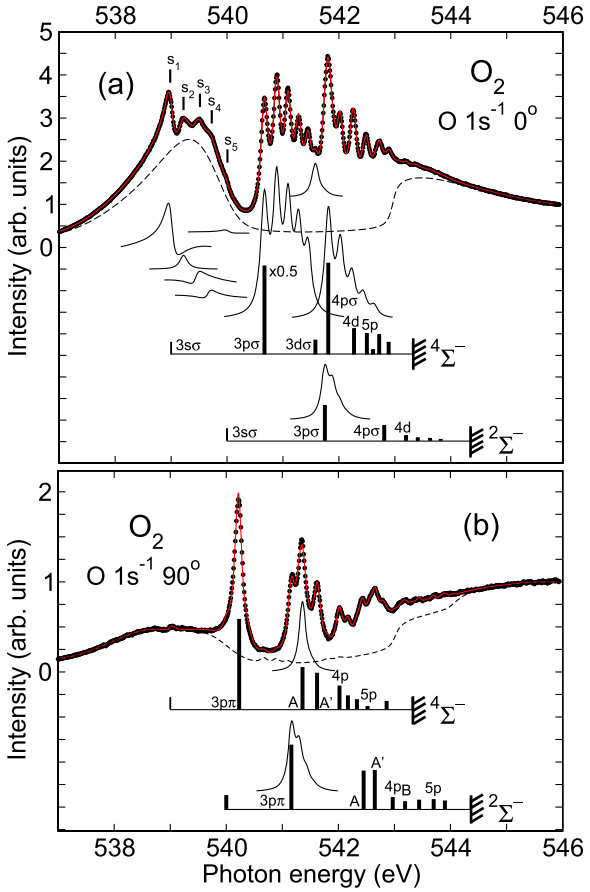

FIG. 2. The angularly resolved partial ion-yield spectrum of O_2 below the O $1s\sigma^{-1}$ ionization threshold measured at an angle of (a) 0° and (b) 90° relative to the polarization of the synchrotron radiation. In both panels the solid lines through the data points represent the fit results and the dashed lines the background; for more details, see text. The subspectra in panel (a) indicate the O $1s\sigma_u^{-1}(^4\Sigma_u^-)3s\sigma_g(^3\Sigma_u^-)$ Rydberg excitation with $v = 0$ to 3 (s_1 to s_4) and the O $1s\sigma_u^{-1}(^2\Sigma_u^-)3s\sigma_g(^3\Sigma_u^-)$ Rydberg excitation (s_5) exhibiting a Fano lineshape as well as vibrational progressions of the O $1s\sigma_g^{-1}(^4\Sigma_g^-)3p\sigma_u(^3\Sigma_u^-)$, O $1s\sigma_g^{-1}(^4\Sigma_g^-)4p\sigma_u(^3\Sigma_u^-)$, O $1s\sigma_u^{-1}(^4\Sigma_u^-)3d\sigma_g(^3\Sigma_u^-)$, and O $1s\sigma_g^{-1}(^2\Sigma_g^-)3p\sigma_u(^3\Sigma_u^-)$ Rydberg states. In panel (b) the subspectra display the O $1s\sigma_u^{-1}(^4\Sigma_u^-)3d\pi_g(^3\Pi_u)$ and O $1s\sigma_g^{-1}(^2\Sigma_g^-)3p\pi_u(^3\Pi_u)$ Rydberg states. The vibrational profiles for the states O $1s\sigma_u^{-1}(^4\Sigma_u^-)3d\sigma_g(^3\Sigma_u^-)$ and O $1s\sigma_g^{-1}(^2\Sigma_g^-)3p\sigma_u(^3\Sigma_u^-)$ in panel (a) as well as those for the states O $1s\sigma_u^{-1}(^4\Sigma_u^-)3d\pi_g(^3\Pi_u)$ and O $1s\sigma_g^{-1}(^2\Sigma_g^-)3p\pi_u(^3\Pi_u)$ in panel (b) are identical to those of the corresponding ion[1] and are used for all higher Rydberg states. The bold vertical bars in both panels represent the energy positions and intensities of the higher Rydberg states. The thin vertical bar in panel (a) and (b) illustrate the energy positions of the O $1s\sigma_u^{-1}(^{4,2}\Sigma_u^-)3s\sigma_g(^3\Sigma_u^-)$ Rydberg excitation.

of this excitation, a number of narrow peaks caused by Rydberg excitations are visible; in Fig. 2(a) they are indicated with vertical bars labeled s_1 to s_5. In this energy region only the Rydberg states O $1s\sigma_u^{-1}(^4\Sigma_u^-)3s\sigma_g(^3\Sigma_u^-)$ and O $1s\sigma_u^{-1}(^2\Sigma_u^-)3s\sigma_g(^3\Sigma_u^-)$ are expected based on theoretical predictions.[6–8,17] For the state O $1s\sigma_u^{-1}(^4\Sigma_u^-)3s\sigma_g(^3\Sigma_u^-)$, Feifel *et al.*[6] report calculated vibrational splittings of ≅250 meV. Because of the calculated intensities of Feifel *et al.*[6] and Velkov *et al.*,[17] the most intense peaks s_1 to s_4 are assigned to vibrational substates of the O $1s\sigma_u^{-1}(^4\Sigma_u^-)3s\sigma_g(^3\Sigma_u^-)$ excitation, while s_5 is assumed to originate from the O $1s\sigma_u^{-1}(^2\Sigma_u^-)3s\sigma_g(^3\Sigma_u^-)$ excitation.

The theoretical studies of Feifel *et al.*[6] and Velkov *et al.*[17] predict an interaction between the dissociative final state O $1s\sigma_g^{-1}(^{2,4}\Sigma_g^-)3\sigma_u^*(^3\Sigma_u^-)$ and the bound Rydberg final state O $1s\sigma_u^{-1}(^{2,4}\Sigma_u^-)3s\sigma_g(^3\Sigma_u^-)$. In particular, the calculations of Velkov *et al.* reproduce the experimental photoabsorption cross section very well. From these calculations the authors conclude a non-adiabatic interaction between the states O $1s\sigma_g^{-1}(^{2,4}\Sigma_g^-)3\sigma_u^*(^3\Sigma_u^-)$ and O $1s\sigma_u^{-1}(^{2,4}\Sigma_u^-)3s\sigma_g(^3\Sigma_u^-)$, i.e., it is an appropriate approach to start from the diabatic curves and to consider the interaction between the states as a small perturbation described with the operator $\mathbf{H_{el}}$ representing the electrostatic interaction.[24,25] This finding of Velkov *et al.* is in full agreement with the first type of Rydberg-valence mixing described above.

In the present case, a continuum of levels for the nuclear motion of the dissociative state O $1s\sigma_g^{-1}(^{2,4}\Sigma_g^-)3\sigma_u^*(^3\Sigma_u^-)$ interact with the discrete vibrational levels of the bound state O $1s\sigma_u^{-1}(^{2,4}\Sigma_u^-)3s\sigma_g(^3\Sigma_u^-)$. Based on this situation, the O $1s\sigma_u^{-1}(^{2,4}\Sigma_u^-)3s\sigma_g(^3\Sigma_u^-)$ states are described in the fit analysis by using Fano lineshapes, which are described from the general point of view in Ref. 26 and in the context of nuclear motions in molecules in Ref. 27. Generally, a cross section including a Fano-lineshape can be described by

$$\sigma_{total} = \frac{(q+\epsilon)^2}{1+\epsilon^2}\sigma_a + \sigma_b \qquad (1)$$

with σ_a (σ_b) being the part of the continuum that interacts (does not interact) with the discrete state. Here σ_a represents the background of the fit analysis in the discussed energy region; it is indicated by the dashed line below 540.5 eV in Fig. 2(a) and matches well the cross section calculated in the two-crossing model by Feifel *et al.*[6] According to their calculation the asymmetric lineshape is due to an avoided level crossing of the resonances O $1s\sigma_g^{-1}(^2\Sigma_g^-)3\sigma_u^*(^3\Sigma_u^-)$ and O $1s\sigma_g^{-1}(^2\Sigma_g^-)3p\sigma_u(^3\Sigma_u^-)$, see above. To simulate this asymmetric structure, two "asymmetric" Gaussian functions located at 538.7 eV and 539.3 eV are employed in the fit approach. The "asymmetric" Gaussian functions are obtained by using a photon-energy dependent width $\tilde{\Gamma}$, i.e., $\tilde{\Gamma} = \tilde{\Gamma}_0 + c \cdot (E - E_0)$ with $\tilde{\Gamma}_0$ being a constant value, c the slope of the widths, E the photon energy, and E_0 the energy value for the maximum of the Gaussian. Although $\tilde{\Gamma}$ and c are free parameters in the fit approach the values are not given since they do not have physical meaning. Furthermore, $\epsilon = 2(E - E_R)/\Gamma$ describes the reduced energy with E_R being the resonance position, Γ the lifetime width, and q the Fano parameter. In the fit analysis it was assumed that the sum of the two cross sections σ_a and σ_b characterizes the excitation O $1s\sigma_g^{-1}(^{2,4}\Sigma_g^-)3\sigma_u^*(^3\Sigma_u^-)$. It was also assumed that for a given vibrational substate the ratio of σ_a to σ_b is independent of the excitation energy.

The five lines labeled s_1 to s_5 are partially overlapping. Because of this, a fit analysis is not unambiguous, in particular since the fit of an individual Fano-lineshape requires the four parameters E_R, Γ, σ_a, and q. To reduce the number of free parameters, we assume in the data analysis identical widths for all resonances. In addition, the energy positions of the first four lines, s_1 to s_4, which are unambiguously assigned to the O $1s\sigma_u^{-1}(^4\Sigma_u^-)3s\sigma_g(^3\Sigma_u^-)$ with $v = 0$ to 3, are described using the formula

$$E_v = E_0 + \hbar\omega(v + \frac{1}{2}). \qquad (2)$$

TABLE I. Summary of the Fano parameters for the O $1s\sigma_u^{-1}(^{2,4}\Sigma_u^-)3s\sigma_g$ $(^3\Sigma_u^-)$ transitions obtained from the fit analysis. The given error bars are the statistical errors obtained within the fit model. All energies are additionally subject to an error of 40 meV due to the calibration of the photon-energy scale.

	Resonance energy (eV)	Assignment	q-parameter
s_1	539.00	O $1s\sigma_u^{-1}(^4\Sigma_u^-)3s\sigma_g(^3\Sigma_u^-)$ ($\nu = 0$)	−1.7(1)
s_2	539.22	O $1s\sigma_u^{-1}(^4\Sigma_u^-)3s\sigma_g(^3\Sigma_u^-)$ ($\nu = 1$)	360(50)
s_3	539.44	O $1s\sigma_u^{-1}(^4\Sigma_u^-)3s\sigma_g(^3\Sigma_u^-)$ ($\nu = 2$)	1.1(3)
s_4	539.66	O $1s\sigma_u^{-1}(^4\Sigma_u^-)3s\sigma_g(^3\Sigma_u^-)$ ($\nu = 3$)	1.3(3)
s_5	540.00	O $1s\sigma_u^{-1}(^2\Sigma_u^-)3s\sigma_g(^3\Sigma_u^-)$ ($\nu = 0$)	−3.5(1.5)

Here, E_ν describes the energy position of the vibrational substate ν, E_0 the minimum of the potential energy curve, and $\hbar\omega$ the vibrational energy. In the fit analysis we also implemented the anharmonicity $x\hbar\omega$. However, since this quantity turned out to result in physically unreasonable values, it was set to $x\hbar\omega = 0$ meV. The results of the fit analysis including the statistical errors are given in Table I.

It is interesting to observe that the q-parameters vary substantially for the different vibrational substates. To understand this we consider the excitation process in a simplified model as presented in Fig. 3. The lower part of the figure shows a harmonic oscillator curve representing the electronic ground state (in the following labeled g) of O_2 together with the wavefunction of the corresponding vibrational ground state, 0_g. The upper part of the figure displays the schematic diabatic curves for the bound Rydberg state O $1s\sigma_u^{-1}(^4\Sigma_u^-)3s\sigma_g(^3\Sigma_u^-)$

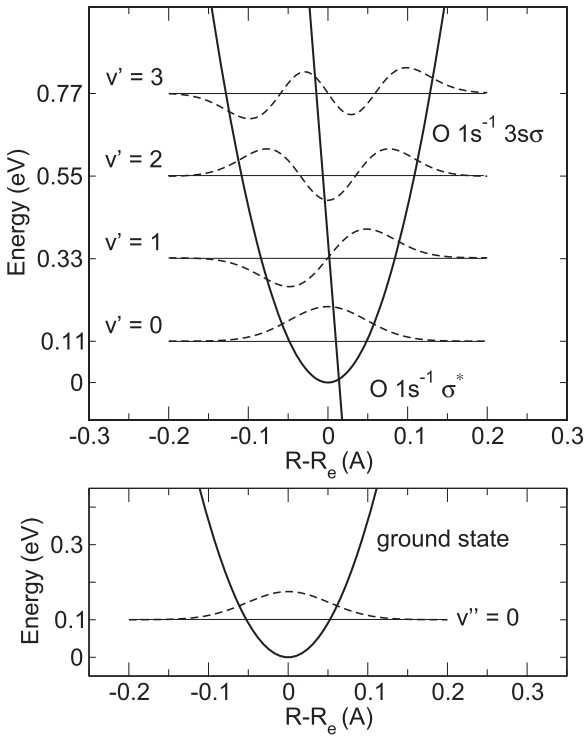

FIG. 3. Simple model to describe the variations of the Fano-parameter q for the vibrational substates of the O $1s\sigma_u^{-1}(^4\Sigma_u^-)3s\sigma_g(^3\Sigma_u^-)$ excitation. The bold solid line in the lower panel describes the schematic potential energy curve of the ground state. The bold solid lines in the upper panel describe the diabatic potential energy curves of the bound core-to-Rydberg excitation and the dissociative core-to-valence excitation. The energy levels (thin horizontal lines) and vibrational wavefunctions (dashed lines) are also shown. For more details, see text.

(labeled b) and the dissociative state O $1s\sigma_g^{-1}(^4\Sigma_g^-)3\sigma_u^*(^3\Sigma_u^-)$ (labeled c for continuum) using a harmonic oscillator potential and a straight line, respectively. For the ground state, a vibrational energy of 200 meV, i.e., a value close to the exact value of 195.9 meV,[28] and for the excited state the present fit result of 220 meV were assumed. The slope of the straight line is taken from the potential energy curve calculated by Velkov *et al.*[17] Its position relative to the bound state was chosen so that its internuclear distances at the energy value of the $\nu = 1$ vibrational level is close to the node of the corresponding vibrational wavefunction; in this way the large Fano-parameter for this vibrational level can be explained, see below. As a consequence of this choice the crossing point of the bound and the dissociative potential energy curve is at an internuclear distance which is by ≅0.015 Å larger than the equilibrium distance of the bound state. This value agrees well with the theoretical results of Feifel *et al.*[6] and Velkov *et al.*[17] The difference in the bond distance of the two bound states of +0.05 Å is arbitrarily chosen and has no influence on the discussion presented below. For the Rydberg state the four lowest vibrational wavefunctions, 0_b to 3_b, are indicated. In this model the Fano-parameter q can be described as[29]

$$q = \frac{1}{\pi}\frac{\langle\Phi_b|\mu|\Phi_g\rangle\langle\chi_b|\chi_g\rangle}{\langle\Phi_c|\mu|\Phi_g\rangle\langle\chi_c|\chi_g\rangle}\frac{1}{\langle\Phi_b|\mathbf{H_{el}}|\Phi_c\rangle\langle\chi_b|\chi_c\rangle}, \quad (3)$$

with Φ and χ being the electronic and the vibrational wave functions, respectively. The quantity μ represents the electronic dipole moment and $\mathbf{H_{el}}$ the operator for the electrostatic interaction between the bound and the continuum state, see above. Since the electronic matrix elements of the diabatic states are identical for all vibrational substates, the Fano-parameter q depends only on the Franck-Condon factors.

Within the *Condon-reflection principle* the vibrational wavefunctions of the dissociative states can be approximated with a δ-function at the classical turning point of the potential.[30] Consequently, the observed lineshape for the dissociative state O $1s\sigma_g^{-1}(^4\Sigma_g^-)3\sigma_u^*(^3\Sigma_u^-)$ is a projection of the vibrational wavefunction $\nu = 0_g$ of the ground state into the energy space by using the potential energy curve of the dissociative state as a mirror, i.e., $\sigma_{dissociative}(E) \propto |\langle\chi_c|\chi_g\rangle|^2$. The matrix element $\langle\chi_c|\chi_g\rangle$ can be considered identical for the energy positions of the different vibrational substates of the transition to the bound state O $1s\sigma_u^{-1}(^4\Sigma_u^-)3s\sigma_g(^3\Sigma_u^-)$ since they are all close to the top of the maximum of the spectral feature caused by the O $1s\sigma_g^{-1}(^4\Sigma_g^-)3\sigma_u^*(^3\Sigma_u^-)$ excitation. This allows to simplify Equation (3) for a qualitative discussion to

$$q \propto \frac{\langle\chi_b|\chi_g\rangle}{\langle\chi_b|\chi_c\rangle}. \quad (4)$$

The absolute values for the overlap matrix element of the vibrational substates in the electronic ground state and in the bound state, $|\langle\chi_b|\chi_g\rangle|$, are for all observable vibrational levels in the same order of magnitude since the intensity is proportional $|\langle\chi_b|\chi_g\rangle|^2$, i.e., to the square of the overlap matrix element which suppresses smaller values for the matrix element significantly. As a consequence the strong variations of q are mainly due to $\langle\chi_b|\chi_c\rangle$, i.e., q is small—and consequently the mixing between the bound and the dissociative state is large—when the matrix element $\langle\chi_b|\chi_c\rangle$ is large and vice

versa. For the present case it means that the mixing between the bound state O $1s\sigma_u^{-1}(^4\Sigma_u^-)3s\sigma_g(^3\Sigma_u^-)$ and the dissociative state O $1s\sigma_g^{-1}(^4\Sigma_g^-)3\sigma_u^*(^3\Sigma_u^-)$ is maximal for the vibrational substates $\nu = 2$ and 3 due to the overlap of the vibrational wavefunctions. In turn the large q for the vibrational substate $\nu = 1$ can be explained with a small overlap between the vibrational wavefunctions $|1_b\rangle$ and $|\chi_c\rangle$, which can be explained with the maximum of the continuum vibrational wavefunction $|\chi_c\rangle$ close to the node of $|1_b\rangle$.

The variations of the signs of the q-values can also be understood within this picture. The overlap between the wavefunction of the vibrational ground state of the electronic ground state, $|0_g\rangle$, and the vibrational wavefunctions of the Rydberg state, $|\nu_b\rangle$, i.e., $\langle\nu_b|0_g\rangle$, changes sign with each increment of the vibrational quantum number ν_b. In the schematic situation displayed in the upper part of Fig. 3, $\langle\chi_c|\nu_b\rangle$ is positive for $\nu = 0$, 1, and 3 but negative for $\nu = 2$. As a result of Eq. (4) follows that q has the same sign for $\nu = 1$, 2, and 3 but a different one for $\nu = 0$. Note that this model does not provide the exact sign of the q-values but only relative signs since (i) the electronic parts of the matrix elements in Eq. (3) and (ii) additional phase factors for 0_g and χ_c can lead to additional factors of -1; these additional factors, however, influence all q-parameters in the same way. In summary, the simple model describes quantitatively the observed variations of the q-parameter and show, in accordance with the expectation for the first type of Rydberg-valence mixing, that a diabatic picture as well as the utilized potential energy curves of the core-excited stats are well suited to describe the interaction between the states O $1s\sigma_u^{-1}(^4\Sigma_u^-)3s\sigma_g(^3\Sigma_u^-)$ and O $1s\sigma_g^{-1}(^4\Sigma_g^-)3\sigma_u^*(^3\Sigma_u^-)$.

2. The O $1s\sigma_g^{-1}$ Ryd excitations

The region above 540.5 eV is dominated by O $1s\sigma_g^{-1}(^4\Sigma_g^-)$ $np\sigma_u(^3\Sigma_u^-)$ and O $1s\sigma_u^{-1}(^4\Sigma_u^-)nd\sigma_g(^3\Sigma_u^-)$ Rydberg states, which are enhanced in their intensity by an interaction due to an avoided level crossing with the dissociative state O $1s\sigma_g^{-1}(^4\Sigma_g^-)3\sigma_u^*(^3\Sigma_u^-)$.[8,9] Both Velkov *et al.*[17] and Feifel *et al.*[6] calculated that the electronic interaction between O $1s\sigma_g^{-1}3\sigma_u^*$ and O $1s\sigma_u^{-1}3s\sigma_g$ is roughly one order of magnitude weaker than between O $1s\sigma_g^{-1}3\sigma_u^*$ and O $1s\sigma_g^{-1}3p\sigma_u$. This can be understood by the fact that in the first case we have the first type of Rydberg-valence mixing described above while in the second case we do have the second type. Following this argument, we expect that the electronic interaction between O $1s\sigma_g^{-1}3\sigma_u^*$ and O $1s\sigma_u^{-1}nd\sigma_g$ is also weak, since this is a type 1 interaction.

In addition to the states converging towards the threshold O $1s\sigma^{-1}(^4\Sigma^-)$, a number of O $1s\sigma_g^{-1}(^2\Sigma_g^-)np\sigma_u(^3\Sigma_u^-)$ and O $1s\sigma_u^{-1}(^2\Sigma_u^-)nd\sigma_g(^3\Sigma_u^-)$ Rydberg states can be found. The energy positions, E, the effective quantum numbers, $n-\delta$, and the quantum defects, δ, of the Rydberg states are summarized in Table II. For the $3p\sigma_u$ Rydberg states, a quantum defect of $\delta \cong 0.7$ and for the higher $np\sigma_u$ Rydberg states of $\delta \cong 1.0$ are observed. For the $nd\sigma_g$ Rydberg states the quantum defect increases from $\delta = 0.22$ for $n = 3$ to $\delta \cong 0.6$ for $n = 5$. Although these values are slightly larger than those observed in the O $1s\sigma^{-1}$ absorption spectra of CO and NO (less than 0.3),[32] they are still in reasonable agreement and support the given assignment.

In the following we shall first describe the principle ideas used for the fit analysis of the vibrational progressions and the background. The ideas are discussed in more detail further below along with the individual spectral features.

All the Rydberg states are described with a Lorentzian lineshape using a width of $\Gamma = 150$ meV full width at half maximum (FWHM) to account for the core-hole lifetime. These lines are convoluted with a Gaussian of 40 meV FWHM to describe the experimental resolution.

The strong avoided level crossing between the O $1s\sigma_g^{-1}$ $(^4\Sigma_g^-)3\sigma_u^*(^3\Sigma_u^-)$ excitation and the O $1s\sigma_g^{-1}(^4\Sigma_g^-)np\sigma_u(^3\Sigma_u^-)$ excitations leads for the low-n Rydberg states to larger equilibrium distances and higher vibrational energies than for unperturbed Rydberg states. Because of this for these excitations individual vibrational progressions are used; they are described in more detail further below. For all other Rydberg states the interaction is much weaker, so that the same vibrational progression as found for the corresponding ion[1] is employed. These vibrational progressions are displayed in Figs. 2(a) and 2(b) and the differences are due to unequal equilibrium distances in the O $1s\sigma^{-1}(^{2,4}\Sigma^-)$ core-ionized states.

In the region of the resolved Rydberg states, the background represented by the dashed line is described with a linear function. As can be seen by the decreasing intensity above 543 eV the unresolved Rydberg states and the continuum are still modified by the interaction with the O $1s\sigma_g^{-1}(^4\Sigma_g^-)3\sigma_u^*(^3\Sigma_u^-)$ state. To describe this behavior the background also consists of a constant value, C, representing the increase of the O $1s^{-1}$ photoionization cross section well above the region of the diabatic O $1s\sigma_g^{-1}(^4\Sigma_g^-)3\sigma_u^*(^3\Sigma_u^-)$ state. The decrease of the cross section above 543 eV is described by a broad Gaussian function, $G(E)$, centered at 543.6 eV. To describe the transition from the resolved to the unresolved Rydberg states the constant background and the Gaussian are multiplied by a sum of arctan-functions, i.e.,

$$I(E) = \sum_e \sum_\nu I_{e\nu}\left(\arctan\frac{E - E_{e\nu}}{\Gamma} + \frac{\pi}{2}\right)\cdot(G(E) + C). \quad (5)$$

Here, e runs over the ionization thresholds $(^2\Sigma^-)$ and $(^4\Sigma^-)$ and ν indicates the different vibrational levels. The quantities $E_{e\nu}$ and $I_{e\nu}$ are the energy position and the relative intensity in the vibrational progression of the ν'th vibrational level of the first unresolved Rydberg state converging to the threshold e.

The above already discussed larger equilibrium distance of the O $1s\sigma_g^{-1}(^4\Sigma_g^-)3p\sigma_u(^3\Sigma_u^-)$ state in comparison to the higher-n Rydberg states can be seen in the long vibrational progression, which is assigned unambiguously by several authors.[8–10] A Franck-Condon fit analysis[32] of this state is not possible since the avoided level crossing results in a dependence of the electronic matrix element on the internuclear distance. Because of this we approximated the vibrational progression by using a Franck-Condon analysis, where the higher substates were suppressed empirically by the factor $f = 1 + a\cdot\nu + b\cdot\nu^2$ with $a = -0.181$ and $b = 0.015$. Furthermore,

TABLE II. The energy positions, E, the effective quantum numbers, $n-\delta$, as well as the splitting, ΔE, of the Rydberg states in the 0° spectrum converging to the thresholds $^2\Sigma^-$ and $^4\Sigma^-$. The error bars for the ionization thresholds result from fitting the energy positions to the Rydberg formula. All energies are additionally subject to an error of 40 meV due to the calibration of the photon-energy scale.

	$^4\Sigma^-$			$^2\Sigma^-$			
Rydberg state	E	$n-\delta$	δ	E	$n-\delta$	δ	ΔE
$3s\sigma_g$	539.00	1.77(1)	1.23(1)	540.00	1.77(1)	1.23(1)	1.00
$3p\sigma_u$	540.67	2.27(2)	0.73(2)	541.75	2.28(2)	0.72(2)	1.08
$3d\sigma_g$	541.58	2.80(2)	0.20(2)				
$4p\sigma_u$	541.81	3.00(3)	1.00(3)	542.81	2.92(3)	1.08(2)	1.00
$4d\sigma_g$	542.27	3.60(5)	0.40(5)	543.20	3.42(4)	0.58(4)	0.93
$5p\sigma_u$	542.50	4.07(7)	0.93(7)	543.41	3.78(6)	1.22(6)	0.91
$5d\sigma_g$	542.61	4.38(10)	0.62(10)	543.63	4.31(9)	0.69(9)	1.02
$6p\sigma_u$	542.72	4.76(13)	1.24(13)	543.82	5.01(15)	0.99(15)	1.10
$7p\sigma_u$	542.89	5.62(22)	1.38(22)				
I_p	543.32(3)			544.36(3)			

we suppressed the vibrational substates with $v \geq 5$ completely since the constant ionic state (CIS) spectra of Piancastelli *et al.*[31] showed that the states O $1s\sigma_g^{-1}(^4\Sigma_g^-)3p\sigma_u(^3\Sigma_u^-)$ and O $1s\sigma_g^{-1}(^4\Sigma_g^-)4p\sigma_u(^3\Sigma_u^-)$ do not overlap. In particular, the CIS spectrum using the final state $1\pi_g^{-1}$ of O_2^+ showed that the intensity between the spectral features related to O $1s\sigma_g^{-1}(^4\Sigma_g^-)3p\sigma_u(^3\Sigma_u^-)$ and O $1s\sigma_g^{-1}(^4\Sigma_g^-)4p\sigma_u(^3\Sigma_u^-)$ is identical to the baseline.

This description of the O $1s\sigma_g^{-1}(^4\Sigma_g^-)3p\sigma_u(^3\Sigma_u^-)$ excitation allows to describe the intensities of the first five vibrational substates quite well and results in an equilibrium distance $R_e = 1.32$ Å and $\hbar\omega = 237$ meV; the equilibrium distance is mainly based on the $v = 0$ to $v = 1$ intensity ratio and the assumption that the electronic matrix element does not show a strong dependence on the internuclear distance close to the minimum of the potential energy curve. The equilibrium distance obtained with the present rough approach agrees surprisingly well with the theoretical value $R_{e,th} \cong 1.30$ Å reported by Feifel *et al.*[6] and Velkov *et al.*[17] The significantly higher value for the vibrational energy than for the corresponding core-ionized state of $\hbar\omega = 180$ meV can readily be understood since the avoided level crossing replaces the inner part of the unperturbed O $1s\sigma_g^{-1}(^4\Sigma_g^-)3p\sigma_u(^3\Sigma_u^-)$ Rydberg state by that of the dissociative O $1s\sigma_g^{-1}(^4\Sigma_g^-)3\sigma_u^*(^3\Sigma_u^-)$ state; the latter one is shifted towards slightly larger internuclear distances and explains the larger equilibrium distance. In contrast to this remains the potential energy curve at internuclear distances larger than the equilibrium distance not affected by the avoided level crossing so that the entire potential energy curve becomes narrower.

In the present work the peak at 541.58 eV is assigned to O $1s\sigma_u^{-1}(^4\Sigma_u^-)3d\sigma_g(^3\Sigma_u^-)$ with $v = 0$, in contrast to the assignment O $1s\sigma_g^{-1}(^4\Sigma_g^-)3p\sigma_u(^3\Sigma_u^-)$ with $v = 5$ of Tanaka *et al.*[10] As described above, we simulated in our fit analysis the vibrational progression of the O $1s\sigma_u^{-1}(^4\Sigma_u^-)3d\sigma_g(^3\Sigma_u^-)$ state with the progression of the O $1s\sigma^{-1}(^4\Sigma^-)$ core ionized state. In addition to the good description of the spectrum within the fit approach the present assignment is supported by the following facts: First, the resulting quantum defect $\delta = 0.20$ is in perfect agreement with the value $\delta = 0.22$ for the O $1s\sigma^{-1}3d\sigma$ excitation of CO.[32] In contrast to this, the assignment of the peak at 542.27 eV to the O $1s\sigma_u^{-1}(^4\Sigma_u^-)3d\sigma_g(^3\Sigma_u^-)$ state as given by Tanaka *et al.*[10] results in $\delta = 1.4$, i.e., a value much larger than expected for $nd\sigma_g$ Rydberg states. Second, as also described above there is a well pronounced minimum between the states O $1s\sigma_g^{-1}(^4\Sigma_g^-)3p\sigma_u(^3\Sigma_u^-)$ and O $1s\sigma_g^{-1}(^4\Sigma_g^-)4p\sigma_u(^3\Sigma_u^-)$ in the CIS spectra of Piancastelli *et al.*[31] These spectra detect the admixing of the O $1s\sigma_g^{-1}(^4\Sigma_g^-)3\sigma_u^*(^3\Sigma_u^-)$ state to the Rydberg states. Consequently, an assignment of the peak at 541.58 eV to an O $1s\sigma_u^{-1}(^4\Sigma_u^-)3d\sigma_g(^3\Sigma_u^-)$ state with only minor admixing of the O $1s\sigma_g^{-1}(^4\Sigma_g^-)3\sigma_u^*(^3\Sigma_u^-)$ state can explain the observed minimum between the states O $1s\sigma_g^{-1}(^4\Sigma_g^-)3p\sigma_u$ $(^3\Sigma_u^-)$ and O $1s\sigma_g^{-1}(^4\Sigma_g^-)4p\sigma_u(^3\Sigma_u^-)$. Third, a fit approach that tries to describe not only the peaks between 540.57 eV and 541.45 eV ($v = 1$–4) but also the peak at 541.58 eV (presumed $v = 5$) as one vibrational progression failed since the energy position of the peak presumed as $v = 5$ does not fit in a vibrational progression described with $E = E_0 + \hbar\omega(v + 0.5) - x\hbar\omega(v + 0.5)^2$.

The vibrational sublevel $v = 0$ of the next transition of this Rydberg series, the O $1s\sigma_g^{-1}(^4\Sigma_g^-)4p\sigma_u(^3\Sigma_u^-)$ transition, is found at an excitation energy of 541.81 eV. The intensities of the higher vibrational substates in the progression of this Rydberg state are considerably lower than for the above discussed state O $1s\sigma_g^{-1}(^4\Sigma_g^-)3p\sigma_u(^3\Sigma_u^-)$. They are, however, still higher than for the O $1s\sigma^{-1}(^4\Sigma^-)$ core-ionized state so we conclude that this state has also admixtures of the O $1s\sigma_g^{-1}(^4\Sigma_g^-)3\sigma_u^*(^3\Sigma_u^-)$ state. The assignment of the vibrational sublevels $v = 0$ and 1 of this vibrational progression is fully confirmed by Sorensen *et al.*[12] using resonant Auger spectra. Although the admixing of the O $1s\sigma_g^{-1}(^4\Sigma_g^-)3\sigma_u^*(^3\Sigma_u^-)$ valence state does not allow to apply a Franck-Condon analysis strictly, we estimated by using the above described assumption on the electronic matrix element from the $v = 0$ to $v = 1$ intensity ratio an equilibrium distance of $R_e \cong 1.27$ Å as well as a vibrational energy of $\hbar\omega = 219(5)$ meV. The smaller equilibrium distance and lower vibrational energy than for the O $1s\sigma_g^{-1}(^4\Sigma_g^-)3p\sigma_u(^3\Sigma_u^-)$ state can easily be explained by the repulsive part of the potential energy curve. This part is also formed by the unperturbed O $1s\sigma_g^{-1}(^4\Sigma_g^-)3\sigma_u^*(^3\Sigma_u^-)$

state; the latter potential energy curve, however, is at smaller internuclear distances due to the higher energy. The higher vibrational substates ($v \geq 2$) are simulated by assuming that the Born-Oppenheimer approximation is valid and serves as an approximation of their contributions to the spectrum.

The peak at 542.27 eV is assigned to the O $1s\sigma_u^{-1}(^4\Sigma_u^-)4d\sigma_g(^3\Sigma_u^-)$ excitation with $v = 0$, which overlaps with the O $1s\sigma_g^{-1}(^4\Sigma_g^-)4p\sigma_u(^3\Sigma_u^-)$ excitation with $v = 2$, see Fig. 2(a). Although the present fit analysis gives only approximate intensities for the higher vibrational substates of the O $1s\sigma_g^{-1}(^4\Sigma_g^-)4p\sigma_u(^3\Sigma_u^-)$ excitation, we can conclude that the vibrational substates ($v = 2$) explain a considerable part of the intensity of the peak under discussion. This also explains the observation of $np\sigma_u$ Rydberg contributions in the resonant Auger spectra taken for this peak.[10] Based on the resonant Auger spectra Tanaka *et al.*[10] assigned the peak at 542.27 eV suggesting a mixing between the O $1s\sigma_u^{-1}(^4\Sigma_u^-)3d\sigma_g(^3\Sigma_u^-)$ and the O $1s\sigma_g^{-1}(^4\Sigma_g^-)4p\sigma_u(^3\Sigma_u^-)$ Rydberg state. Both the $1s\sigma_u^{-1}(^4\Sigma_u^-)3d\sigma_g(^3\Sigma_u^-)$ excitation and the O $1s\sigma_g^{-1}(^4\Sigma_g^-)4p\sigma_u(^3\Sigma_u^-)$ excitation have an *ungerade* symmetry of the total wavefunction and can, in principle, mix. However, they differ by two orbitals so that the mixing of these two Rydberg states is analogous to the first type of Rydberg-valence mixing, which is very weak. In the present case the potential energy curves of the excited states are well separated by about two vibrational quanta. Furthermore, two Rydberg orbitals are spatially more extended and overlap less than a Rydberg orbital with a valence orbital. Because of this we expect that mixing between these states is much smaller than in case of Rydberg-valence mixing and, therefore, negligible.

As already discussed above, within our fit analysis the O $1s\sigma_u^{-1}(^4\Sigma_u^-)4d\sigma_g(^3\Sigma_u^-)$ Rydberg state, as well as all higher Rydberg states converging to the O $1s\sigma^{-1}(^4\Sigma^-)$ ionization threshold, namely O $1s\sigma_g^{-1}(^4\Sigma_g^-)5p\sigma_u(^3\Sigma_u^-)$ to O $1s\sigma_g^{-1}(^4\Sigma_g^-)7p\sigma_u(^3\Sigma_u^-)$ and O $1s\sigma_u^{-1}(^4\Sigma_u^-)3d\sigma_g(^3\Sigma_u^-)$ to O $1s\sigma_u^{-1}(^4\Sigma_u^-)5d\sigma_g(^3\Sigma_u^-)$, are simulated using the same vibrational progression as observed for the core-ionized state. Since the simulated vibrational progressions describe the spectrum well, we assume that the corresponding states have only small admixing of the O $1s\sigma_g^{-1}(^4\Sigma_g^-)3\sigma_u^*(^3\Sigma_u^-)$ state. As a consequence, the influence of the admixing on the vibrational progression can be neglected. There is, however, still the already described influence on the intensity as can be seen by the background above 543 eV, which describes the unresolved higher Rydberg states as well as the ionization continuum. The background decreases continuously from 543 eV to 545 eV in full agreement with the theoretical absorption spectrum in the diabatic model,[6] i.e., it is governed by the intensity of the O $1s\sigma_g^{-1}(^4\Sigma_g^-)3\sigma_u^*(^3\Sigma_u^-)$ state.

Since the interaction between the O $1s\sigma^{-1}(^2\Sigma^-)Ryd(^3\Sigma_u^-)$ states and the O $1s\sigma_g^{-1}(^4\Sigma_g^-)3\sigma_u^*(^3\Sigma_u^-)$ state is expected to be very small,[17] the intensity of these Rydberg excitations is smaller than for the O $1s\sigma^{-1}(^4\Sigma^-)Ryd(^3\Sigma_u^-)$ states. With the same argument the vibrational progressions of all O $1s\sigma^{-1}(^2\Sigma^-)Ryd(^3\Sigma_u^-)$ states can be simulated using those observed for the core ionized state.[1] In this way, we found between the observed O $1s\sigma^{-1}(^2\Sigma^-)Ryd(^3\Sigma_u^-)$ excitations and the corresponding O $1s\sigma^{-1}(^4\Sigma^-)Ryd(^3\Sigma_u^-)$ states energy splittings that are close to the value of ≅ 1.04 eV observed for the photoionization thresholds, see Table II.

The excitations O $1s\sigma_g^{-1}(^2\Sigma_g^-)3p\sigma_u(^3\Sigma_u^-)$ with $v = 0$ and O $1s\sigma_g^{-1}(^4\Sigma_g^-)4p\sigma_u(^3\Sigma_u^-)$ with $v = 0$ overlap almost perfectly according to the present fit analysis, so that there is no obvious indication for such an assignment. However, there are three arguments which support the present fit result. First, a closer inspection of the peak at ≅541.8 eV shows that it is broader than those peaks which are predominantly assigned to individual transitions. Second, both Feifel *et al.*[6] and Velkov *et al.*[17] predict an enhancement of the intensity for the O $1s\sigma_g^{-1}(^2\Sigma_g^-)3p\sigma_u(^3\Sigma_u^-)$ transition due to an interaction with the O $1s\sigma_g^{-1}(^4\Sigma_g^-)3\sigma_u^*(^3\Sigma_u^-)$ state. Third, the resonant Auger spectrum of Tanaka *et al.*[10] taken at 541.80 eV shows rather strong contributions of transitions to $3p\sigma_u$ final states. These contributions would require an unexpected strong shake-down effect in the resonant Auger decay if the peak at 541.8 eV was due to the O $1s\sigma_g^{-1}(^4\Sigma_g^-)4p\sigma_u(^3\Sigma_u^-)$ state with $v = 0$ alone.

B. The 90° spectrum

Fig. 2(b) shows the 90° spectrum including the fit result, which is represented by the solid lines through the data points. The fit is performed in a similar way to the 0° spectrum, i.e., the vibrational progressions used to describe the Rydberg states are identical to those of the corresponding ion. The background consists of a linear part, two broad Gaussians to describe the O $1s\sigma_g^{-1}3\sigma_u^*(^3\Sigma_u^-)$ state and a number of arctan-functions to describe the unresolved Rydberg states and the continuum. In addition, several weak Lorentzian lineshapes are included in the spectrum. Their energy positions are identical to the most intense lines in the 0° spectrum and we assume that their origin is mostly due to a finite acceptance angle of the ion detectors.

It is expected that the 90° spectrum has a simpler structure than the 0° spectrum since based on the assumption that the projection of the orbital angular momentum on the molecular axis, Λ, is a good quantum number only excitations into orbitals with Π symmetry are expected, see above. These selection rules for the photoabsorption are in the present angularly resolved ion-yield technique only applicable if the axial recoil approximation is valid, i.e., the molecule does not rotate on the time scale of dissociation. However, breakdown of the axial recoil approximation has been found, e.g., for the angular distribution of ionic fragments from some of the Auger final states of CO.[33,34] It has been explained with the metastable dicationic states that hold a vibrational structure and lead to delayed dissociation.

Although the selection rules of Λ explain most of the intensity visible in this spectrum of O_2, we shall show in the following that they are not strictly valid for the 90° spectrum due to a partial breakdown of the axial recoil approximation. This can be, for example, expected for some of the resonant Auger final states that hold vibrational structure[13] populated via the O $1s\sigma_g^{-1}3\sigma_u^*$ excitation. Moreover, van der Kampen *et al.*[35] reported some $n = 3, 4$ Rydberg states in O_2^+, i.e., the most likely final states of the resonant Auger decay of core-to-Rydberg excitations which are metastable as well. Finally, the

kinetic energy release spectrum of O_2^{2+} shows very rich vibrational structures;[36] the latter states posses potential energy curves similar to those of the $n = 3$, 4 Rydberg states in O_2^+. In summary, there is significant evidence for metastable final states in the resonant Auger decay of O_2 so that the axial-recoil approximation is not valid subsequent to some of the resonant Auger transitions. Since the present measurements are a summation over all resonant Auger transitions, it can be understood that the election rules for Λ are not strictly valid as well.

The breakdown of the axial-recoil approximation and as a consequence the not strictly applicable selection rules for Λ can, e.g., be seen by the observation of the broad spectral feature assigned to the O $1s\sigma_g^{-1}3\sigma_u^*(^3\Sigma_u^-)$ core-to-valence excitation. It has a considerable contribution to the spectrum (about 10% of the intensity in the 0° spectrum), which is in contradiction to selection rules based on Λ. This broad feature is also present in the angularly resolved spectra of previous studies[9,10] but has never drawn attention. Because of the following reasons, we can rule out that a large acceptance angle of the ion detector or incomplete polarization is responsible for this finding: (i) The vibrational substates $v = 0$ and 1 of the Rydberg states O $1s\sigma_g^{-1}(^4\Sigma_g^-)3p\sigma_u(^3\Sigma_u^-)$ and O $1s\sigma_g^{-1}(^4\Sigma_g^-)4p\sigma_u(^3\Sigma_u^-)$, which are the most intense peaks in the 0° spectrum (see above), vanish almost completely in the 90° spectrum; their contributions lead to very weak narrow structures included in the background, see dashed line. (ii) The lineshape of the O $1s\sigma_g^{-1}3\sigma_u^*(^3\Sigma_u^-)$ resonance is different in the 0° and in the 90° spectrum. Actually, the shape of the O $1s\sigma_g^{-1}3\sigma_u^*(^3\Sigma_u^-)$ in the 0° spectrum matches quite well the calculated quartet channel, i.e., O $1s\sigma_g^{-1}(^4\Sigma_g^-)3\sigma_u^*(^3\Sigma_u^-)$, of Velkov *et al.* (red line in Fig. 3 of Ref. 17) while its shape in the 90° spectrum matches much better the calculated doublet channel, i.e., O $1s\sigma_g^{-1}(^2\Sigma_g^-)3\sigma_u^*(^3\Sigma_u^-)$ (green line in Fig. 3 of Ref. 17).

For a detailed understanding of the resonances, a fit analysis of the spectrum was performed. Fits for the narrow structure at 540.23 eV assigned to O $1s\sigma_g^{-1}(^4\Sigma_g^-)3p\pi_u(^3\Pi_u)$, see below, are not satisfactory if only one single Lorentzian lineshape is applied. Instead, good results can be obtained with two different fit approaches. In the first approach, a Fano-lineshape with a q-parameter of 16(5) is used. This approach would indicate an interaction of a discrete state with a continuum state, and it would suggest an interaction of the bound O $1s\sigma_g^{-1}(^4\Sigma_g^-)3p\pi_u(^3\Pi_u)$ Rydberg state with the O $1s\sigma_g^{-1}(^2\Sigma_g^-)3\sigma_u^*(^3\Sigma_u^-)$ core-to-valence excitation, which is the only dissociative state in this energy region. However, such a mixing of states with different Λ would require a spin-orbit interaction which is known to be very small in O_2[38] so this explanation is rather doubtful. In the second approach an additional vibrational progression of low intensity is fitted in the energy region below the spectral feature at 540.23 eV. This results in an excitation energy of 540.00 eV for the additional structure suggesting that the O $1s\sigma_u^{-1}(^2\Sigma_u^-)3s\sigma_g(^3\Sigma_u)$ state is also present in the 90° spectrum due to a violation of the axial-recoil approximation.

In addition to the O $1s\sigma_u^{-1}(^2\Sigma_u^-)3s\sigma_g(^3\Sigma_u)$ state, we observed at 539.00 eV a weak Fano-lineshape which is assigned to the O $1s\sigma_u^{-1}(^4\Sigma_u^-)3s\sigma_g(^3\Sigma_u)(v = 0)$ state. Obviously for both the O $1s\sigma_u^{-1}3s\sigma_g$ and the O $1s\sigma_g^{-1}3\sigma_u^*$ configuration the $(^2\Sigma^-)$ component is in the 90° spectrum stronger than the $(^4\Sigma^-)$ component. This suggests that the resonant Auger decays of the $(^2\Sigma^-)$ components lead to a stronger population of final states which allow rotation of the molecule prior to dissociation. At least for the O $1s^{-1}$ Rydberg state this behavior can be understood qualitatively by different equilibrium distances of the components $(^4\Sigma^-)$ and $(^2\Sigma^-)$, see above, so that different vibrational levels of the final states are populated. Such differences in the population of vibrational levels were shown in detail for the O $1s^{-1}(^4\Sigma^-)$ and O $1s^{-1}(^2\Sigma^-)$ core-ionized states by Arion *et al.*[37]

In the fit approaches the O $1s\sigma_g^{-1}(^4\Sigma_g^-)3p\pi_u$ $(^3\Pi_u)$ Rydberg state at 540.23 eV has been described successfully with a vibrational progression similar to that of the corresponding ion. Because of this we simulated the vibrational progressions of the Rydberg states converging towards the O $1s\sigma^{-1}(^4\Sigma^-)$ and O $1s\sigma^{-1}(^2\Sigma^-)$ ionization thresholds on the basis of the corresponding equilibrium distances and vibrational energies

TABLE III. The energy positions, E, the effective quantum numbers, $n-\delta$, as well as the splitting, ΔE, of Rydberg states in the 90° spectrum converging to the thresholds $^2\Sigma^-$ and $^4\Sigma^-$. The error bars for the ionization thresholds result from fitting the energy positions to the Rydberg formula. All energies are additionally subject to an error of 40 meV due to the calibration of the photon-energy scale.

	$^4\Sigma^-$			$^2\Sigma^-$			
Rydberg state	E	$n-\delta$	δ	E	$n-\delta$	δ	ΔE
$3p\pi_u$	540.23	2.10(1)	0.90(1)	541.16	2.06(1)	0.94(1)	0.93
A	541.36	2.63(2)	0.37(2)	542.45	2.67(2)	0.33(2)	1.09
$A'(n = 3)$	541.62	2.83(3)	0.17(3)	542.65	2.82(3)	0.18(3)	1.03
$A'(n = 4)$	541.62	1.83(3)	1.17(3)	542.65	1.82(3)	1.18(3)	1.03
$4p\pi_u$	542.02	3.23(4)	0.77(4)	542.97	3.13(4)	0.87(4)	0.95
B	542.17	3.44(5)	0.56(5)	543.19	3.41(4)	0.59(4)	1.02
$B'(n = 4)$	542.33	3.71(6)	0.29(6)	543.44	3.84(7)	0.16(7)	1.11
$B'(n = 5)$	542.33	2.71(6)	1.29(6)	543.44	2.84(7)	1.16(7)	1.11
$5p\pi_u$	542.52	4.12(8)	0.88(8)	543.70	4.54(11)	0.46(11)	1.18
$6p\pi_u$	542.86	5.43(20)	0.57(20)	543.90	5.43(20)	0.57(20)	1.04
I_p	543.32(3)			544.36(3)			

for the core ionized states given by Sorensen *et al.*[1] In this way an excellent description of the experimental spectrum was obtained using eight pairs of states, all with a splitting close to 1.04 eV, i.e., close to the splitting between the two ionization thresholds O $1s\sigma^{-1}(^4\sum^-)$ and O $1s\sigma^{-1}(^2\sum^-)$. The fit results of these eight pairs of states including the energy positions and quantum defects δ are summarized in Table III. Using I_p = 543.30(3) eV for the O $1s\sigma^{-1}(^4\sum^-)$ ionization threshold as obtained from fits of the Rydberg series $np\sigma$ and $nd\sigma$ in the 0° spectrum, see below, the states can be assigned to three different series.

Based on the assumption that Λ is a good quantum number, only series with Π-symmetry, namely O $1s\sigma_g^{-1}np\pi_u$, O $1s\sigma_u^{-1}nd\pi_g$, O $1s\sigma_g^{-1}nf\pi_u$ and so on are expected to converge towards each of the two ionization thresholds O $1s\sigma^{-1}(^4\sum^-)$ and O $1s\sigma^{-1}(^2\sum^-)$. The series $np\pi_u$ can readily be assigned based on its quantum defect $\delta \cong 0.9$; this assignment has been fully confirmed by resonant Auger spectra.[10] The assignment of the remaining two series is more difficult.

The series O $1s\sigma^{-1}nf\pi$ is expected to be weak and has not been observed in the photoabsorption spectra below the $1s\sigma$ ionization threshold of other molecules like CO or NO.[9,32,39,40] In addition, an assignment of one of these series to the $nf\pi_u$ Rydberg series would result in a quantum defect $\delta \cong 1.2 - 1.4$, which is in contradiction to the expectation of a quantum defect close to 0. Because of this, an assignment of one of the series to $nf\pi_u$ is not convincing. Kosugi *et al.*[7] pointed out that there are two additional states in a configuration O $1s\sigma^{-1}1\pi^{*2}nl\pi^1$ which have $^3\Pi$ symmetry, namely those where the 2 electrons in the open valence shell $1\pi^*$ couple to $^1\Delta_g$ and a $^1\sum_g^+$. However, Kosugi *et al.*[7] also pointed out that their configuration mixing with the two dipole allowed states $1s\sigma^{-1}(^{4,2}\sum^-)1\pi^{*2}(^3\sum^-)nl\pi^1(^3\Pi)$ is very small, resulting in no transition probability. Based on these arguments only the O $1s\sigma_u^{-1}(^{4,2}\sum^-)1\pi^{*2}(^3\sum^-)nd\pi_g(^3\Pi)$ series are expected in the spectrum, contrary to the observation of two different series. Since the following discussion will not result into a unambiguous assignment, we label the two pairs of states lower in energy to A and A' as well as those higher in energy to B and B'.

Based on the above discussed breakdown of the axial-recoil approximation the series $nd\sigma_g$ and $ns\sigma_g$ can contribute to the 90° spectrum. For the latter series the states with $n \geq 4$ are not observed in the 0° spectrum, but they might only be masked by the much more intense series $np\sigma_u$ and $nd\sigma_g$. In the following we shall first discuss an assignment based on the series $nd\pi_u$ and $ns\sigma_g$ followed by an assignment based on $nd\pi_u$ and $nd\sigma_g$.

In an approach based on the series $nd\pi_u$ and $ns\sigma_g$, A' can be assigned to O $1s\sigma_u^{-1}4s\sigma_g(^3\sum_u^-)$ and B' to O $1s\sigma_u^{-1}5s\sigma_g(^3\sum_u^-)$, both with a quantum defect of $\delta \cong 1.2$, i.e., a value very close to that observed for O $1s\sigma_u^{-1}3s\sigma_g(^3\sum_u^-)$. As a consequence A and B would form the expected series $nd\pi_g$ with n = 3,4. This approach to the assignment is, however, not conclusive since it is based on states $ns\sigma_g$ that are too weak to be observed in the 0° spectrum.

An assignment based on the series $nd\pi_u$ and $nd\sigma_g$ has to take into account the energy positions of the energy positions of the latter series obtained in the 0° spectrum. The state $(^4\sum^-)A'$ observed at 541.62 eV coincides within the error bars with the O $1s\sigma_u^{-1}(^4\sum_u^-)3d\sigma_g$ $(^3\sum_u^-)$ state observed in the 0° spectrum at 541.58 eV. The same holds for the state $(^2\sum^-)B$ at 543.19 eV that agrees well with the O $1s\sigma_u^{-1}(^2\sum_u^-)4d\sigma_g$ $(^3\sum_u^-)$ state at 543.20 eV in the 0° spectrum. Following the assignment one results with increasing energy in the sequence $3d\pi_d$ (A) followed by $3d\sigma_g$ (A') and in $4d\sigma_g$ (B) by $4d\pi_u$ (B'), i.e., a change in the $d\pi_u/d\sigma_g$ order. In addition to the change in the sequence this assignment leads also to a energy difference of 100 meV between the O $1s\sigma_u^{-1}(^4\sum_u^-)4d\sigma_g$ in the 0° and the 90° spectrum. Because of these observations the assignment is also not conclusive.

Moreover, for both discussed assignments the violation of the axial-recoil approximation is equally strong for the doublet and the quartet component of each configuration since they show similar intensity in the spectra. This would be different from the findings for the configurations O $1s\sigma_u^{-1}3s\sigma_g$ and O $1s\sigma_g^{-1}3\sigma_u^*$, see above, so that the results do not give a completely uniform picture, i.e., a final assignment of the states A, A', B, and B' cannot be given in the present work.

Interestingly, a significant breakdown of the axial-recoil approximation occurs only for the $ns\sigma_g$ and the $nd\sigma_g$ Rydberg series. Contrary to this the most intense Rydberg series $np\sigma_u$ contributes only with very weak structures in the 90° spectrum. This suggests that the decay pathways for the various Rydberg series are significantly different.

Finally we want to point out that it is not surprising that the absence of states with $\sum$-symmetry in the 0° spectrum can be explained with the larger photoabsorption cross section for the $\sum$-states, see intensity scale in Fig. 2, masking possible weak contributions.

III. SUMMARY AND CONCLUSIONS

The photoabsorption spectrum of O_2 below the O $1s\sigma^{-1}$ threshold has been reanalyzed by using a sophisticated fit approach. In the ion-yield spectrum measured at 0° spectrum, Fano-lineshapes were observed for different vibrational substates of the O $1s\sigma_u^{-1}(^4\sum_u^-)3s\sigma_g(^3\sum_u^-)$ excitation indicating an interaction with the O $1s\sigma_g^{-1}(^4\sum_g^-)3\sigma_u^*(^3\sum_u^-)$ state. The different vibrational substates exhibit a strong variation of the Fano-parameter q, which is explained qualitatively with a simple model.

The presence of the states with $\sum$-symmetry belonging to the configurations O $1s\sigma_g^{-1}3\sigma_u^*$, O $1s\sigma_u^{-1}ns\sigma_g$, and O $1s\sigma_u^{-1}nd\sigma_g$ in the O $1s\sigma^{-1}$ partial ion-yield spectrum at 90° shows that the selection rules for the orbital angular momentum Λ are not strictly valid. This is explained with a breakdown of the axial-recoil approximation due to resonant Auger decays to metastable final states which allow the molecule to rotate prior to dissociation. We would like to point out that other diatomic molecules formed by second-row elements like CO, NO, and N_2 posses as well metastable final states that are populated in the resonant Auger decay, so that the prerequisite for a breakdown of the axial-recoil approximation is given. However, contrary to O_2 the corresponding partial ion-yield spectra exhibit only transitions that can be explained with the selection rules for Λ.[9]

ACKNOWLEDGMENTS

We are grateful to Dr. Catalin Miron and Dr. Christophe Nicolas for providing us with the high-resolution total-ion-yield spectra measured at the PLEIADES beamline at the SOLEIL Synchrotron, France during in-house beamtime (Proposal No. 99110017). Furthermore, we gratefully acknowledge initializing contributions of the late Professor Dr. U. Becker in the early stage of this work. The analysis at the Freie Universität Berlin was supported by the Deutsche Forschungsgemeinschaft under Project No. PU180/6-1. R.P. gratefully acknowledges fruitful discussions with Professor Dr. N. Schwentner.

[1] S. L. Sorensen, K. J. Børve, R. Feifel, A. de Fanis, and K. Ueda, J. Phys. B **41**, 095101 (2008).
[2] G. R. Wight and C. E. Brion, J. Electron Spectrosc. Relat. Phenom. **4**, 313 (1974).
[3] R. E. LaVilla, J. Chem. Phys. **63**, 2733 (1975).
[4] A. P. Hitchcock and C. E. Brion, J. Electron Spectrosc. Relat. Phenom. **18**, 1 (1980).
[5] Y. Ma, C. T. Chen, G. Meigs, K. Randall, and F. Sette, Phys. Rev. A **44**, 1848 (1991).
[6] R. Feifel, Y. Velkov, V. Carravetta, C. Angeli, R. Cimiraglia, P. Salek, F. Gel'mukhanov, S. L. Sorensen, M. N. Piancastelli, A. De Fanis, K. Okada, M. Kitajima, T. Tanaka, H. Tanaka, and K. Ueda, J. Chem. Phys. **128**, 064304 (2008).
[7] N. Kosugi, E. Shigemasa, and A. Yahishita, Chem. Phys. Lett. **190**, 481 (1992).
[8] A. Yagishita, E. Shigemasa, and N. Kosugi, Phys. Rev. Lett. **72**, 3961 (1994).
[9] J. Adachi, N. Kosugi, and A. Yagishita, J. Phys. B **38**, R127 (2005).
[10] T. Tanaka, R. Feifel, M. Kitajima, H. Tanaka, S. L. Sorensen, R. Sankari, A. De Fanis, M.-N. Piancastelli, L. Karlsson, and K. Ueda, Phys. Rev. A **78**, 022516 (2008).
[11] M. Neeb, J.-E. Rubensson, M. Biermann, and W. Eberhardt, Phys. Rev. Lett. **71**, 3091 (1993).
[12] S. Sorensen, T. Tanaka, R. Feifel, J. H. D. Eland, M. Kitajima, H. Tanaka, R. Sankari, A. De Fanis, M. N. Piancastelli, L. Karlsson, and K. Ueda, Chem. Phys. Lett. **398**, 168 (2004).
[13] R. Feifel, T. Tanaka, M. Kitajima, H. Tanaka, A. De Fanis, R. Sankari, L. Karlsson, S. Sorensen, M.-N. Piancastelli, G. Prümper, U. Hergenhahn, and K. Ueda, J. Chem. Phys. **126**, 174304 (2007).
[14] A. Lindblad, V. Kimberg, J. Söderström, C. Nicolas, O. Travnikova, N. Kosugi, F. Gel'mukhanov, and C. Miron, New J. Phys. **14**, 113018 (2012).
[15] A. Pietzsch, Y.-P. Sun, F. Hennies, Z. Rinkevicius, H. O. Karlsson, T. Schmitt, V. N. Strocov, J. Andersson, B. Kennedy, J. Schlappa, A. Föhlisch, J.-E. Rubensson, and F. Gel'mukhanov, Phys. Rev. Lett. **106**, 153004 (2011).
[16] V. Kimberg, T. Gejo, M. Oura, T. Tokushima, Y. Horikawa, H. Arai, S. Shin, and N. Kosugi, Phys. Rev. A **85**, 032503 (2012).
[17] Y. Velkov, V. Kimberg, N. Kosugi, R. Salek, and F. Gel'mukhanov, Chem. Phys. Lett. **476**, 147 (2009).
[18] C. Miron *et al.*, PLEIADES, http://www.synchrotron-soleil.fr/portal/page/portal/Recherche/LignesLumiere.
[19] O. Travnikova, J.-C. Liu, A. Lindblad, C. Nicolas, J. Söderström, V. Kimberg, F. Gel'mukhanov, and C. Miron, Phys. Rev. Lett. **105**, 233001 (2010).
[20] J. Söderström, A. Lindblad, A. Grum-Grzhimailo, O. Travnikova, C. Nicolas, S. Svensson, and C. Miron, New J. Phys. **13**, 073014 (2011).
[21] C. Miron, C. Nicolas, O. Travnikova, P. Morin, Y. P. Sun, F. Gelukhanov, N. Kosugi, and V. Kimberg, Nat. Phys. **8**, 135–138 (2012).
[22] V. Kimberg, A. Lindblad, J. Söderström, O. Travnikova, C. Nicolas, Y. P. Sun, F. Gel'mukhanov, N. Kosugi, and C. Miron, Phys. Rev. X **3**, 011017 (2013).
[23] N. Saito, K. Ueda, M. Simon, K. Okada, Y. Shimizu, H. Chiba, Y. Senba, H. Okumura, H. Ohashi, Y. Tamenori, S. Nagaoka, A. Hiraya, H. Yoshida, E. Ishiguro, T. Ibuki, I. H. Suzuki, and I. Koyano, Phys. Rev. A **62**, 042503 (2000).
[24] H. Lefebvre-Brion and R. W. Field, *The Spectra and Dynamics of Diatomic Molecules* (Elsevier, San Diego, CA, 2004), p. 310.
[25] A. W. Jasper, C.-Y. Zhu, S. Nangia, and D. G. Truhlar, Faraday Discuss. **127**, 1 (2004).
[26] U. Fano, Phys. Rev. **124**, 1866 (1961).
[27] See Ref. 24, p. 522.
[28] G. Herzberg, *Molecular Spectra and Molecular Structure I. Spectra of Diatomic Molecules* (Van Nostrand, New York, 1950), p. 560.
[29] M. Chergui, N. Schwentner, and V. Chandrasekharan, Phys. Rev. Lett. **66**, 2499 (1991).
[30] See Ref. 28, p. 392.
[31] M. N. Piancastelli, A. Kivimäki, V. Carravetta, I. Cacelli, R. Cimiraglia, C. Angeli, H. Wang, M. Coreno, M. de Simone, G. Turri, and K. C. Prince, Phys. Rev. Lett. **88**, 243002 (2002).
[32] R. Püttner, I. Dominguez, T. J. Morgan, C. Cisneros, R. F. Fink, E. Rotenberg, T. Warwick, M. Domke, G. Kaindl, and A. S. Schlachter, Phys. Rev. A **59**, 3415 (1999).
[33] T. Weber, O. Jagutzki, M. Hattass, A. Staudte, A. Nauert, L. Schmidt, M. H. Prior, A. L. Landers, A. Bräuning-Demian, H. Bräuning, C. L. Cocke, T. Osipov, I. Ali, R. Díez Muiño, D. Rolles, F. J. García de Abajo, C. S. Fadley, M. A. Van Hove, A. Cassimi, H. Schmidt-Böcking, and R. Dörner, J. Phys. B **34**, 3669 (2001).
[34] T. Weber, M. Weckenbrock, M. Balser, L. Schmidt, O. Jagutzki, W. Arnold, O. Hohn, M. Schöffler, E. Arenholz, T. Young, T. Osipov, L. Foucar, A. De Fanis, R. R. Díez Muiño, H. Schmidt-Böcking, C. L. Cocke, M. H. Prior, and R. Dörner, Phys. Rev. Lett. **90**, 153003 (2003).
[35] A. B. van der Kamp, R. S. Hiemstra, W. J. van der Zande, R. Fink, and M. Jungen, J. Chem. Phys. **99**, 7487 (1993).
[36] M. Lundqvist, D. Edvardsson, P. Baltzer, M. Larsson, and B. Wannberg, J. Phys. B **29**, 499 (1996).
[37] T. Arion, R. Püttner, C. Lupulescu, R. Ovsyannikov, M. Förstel, G. Öhrwall, A. Lindblad, K. Ueda, S. Svensson, A. M. Bradshaw, W. Eberhardt, and U. Hergenhahn, J. Electron Spectrosc. Relat. Phenom. **185**, 234 (2012).
[38] L. Veseth and A. Lofthus, Mol. Phys. **27**, 511 (1974).
[39] M. Domke, C. Xue, A. Puschmann, T. Mandel, E. Hudson, D. A. Shirley, and G. Kaindl, Chem. Phys. Lett. **173**, 122 (1990).
[40] G. Remmers, M. Domke, A. Puschmann, T. Mandel, G. Kaindl, E. Hudson, and D. A. Shirley, Chem. Phys. Lett. **214**, 241 (1993).